1-19-2022

Near-infrared unsymmetrical squaraine core-based sensitizers for co-sensitized high-photocurrent dye-sensitized solar cells

Jonathon Watson
University of Mississippi

Roberta R. Rodrigues
University of Mississippi

Jared H. Delcamp
University of Mississippi

Recommended Citation

Watson, J., Rodrigues, R. R., & Delcamp, J. H. (2022). Near-infrared unsymmetrical squaraine core-based sensitizers for co-sensitized high-photocurrent dye-sensitized solar cells. Cell Reports Physical Science, 3(1), 100701. https://doi.org/10.1016/j.xcrp.2021.100701

Cell Reports
Physical Science

CellPress
OPEN ACCESS

Article

Near-infrared unsymmetrical squaraine core-based sensitizers for co-sensitized high-photocurrent dye-sensitized solar cells

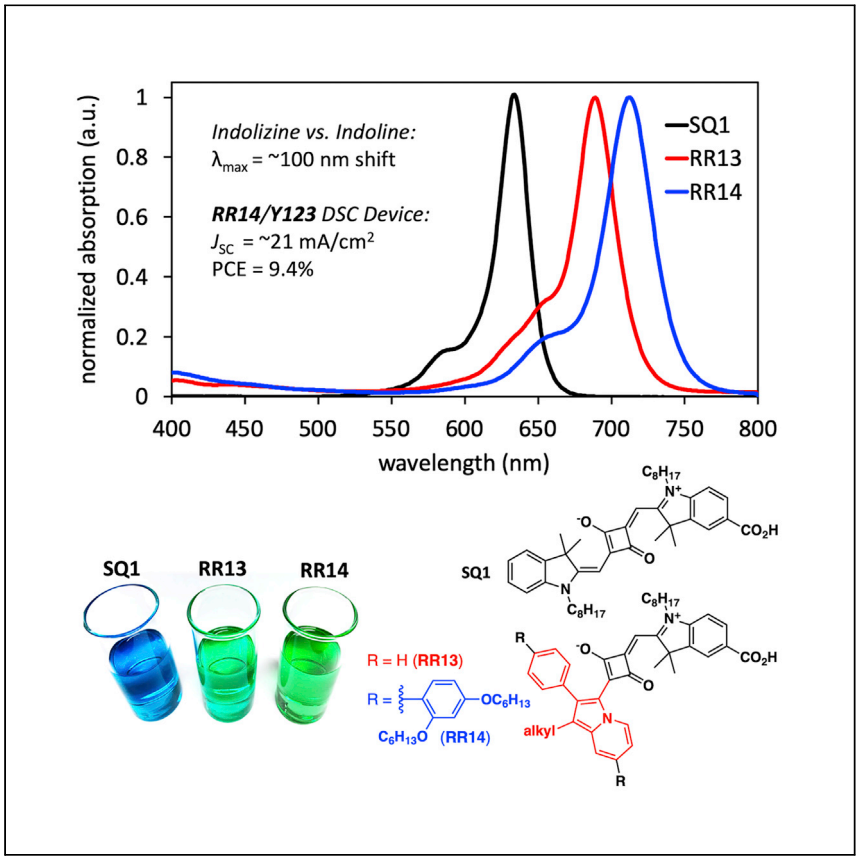

Watson et al. report the design, synthesis, and characterization of unsymmetrical core indolizine-squaraine-indoline dyes to improve short-circuit current density in solar cells. The use of a bulky indolizine donor design broadens NIR photon use in solar cell devices and reduces charge recombination pathways.

Jonathon Watson, Roberta R. Rodrigues, Jared H. Delcamp

delcamp@olemiss.edu

Highlights

NIR unsymmetrical indolizine-squaraine-indoline core dyes are synthesized

Unsymmetrical squaraine dyes improve J_{SC} in DSC devices

Co-sensitized DSC devices with squaraine dyes have increased PCEs

A bulky indolizine donor design increases photoinduced charge separation lifetimes

Watson et al., Cell Reports Physical Science 3, 100701
January 19, 2022
https://doi.org/10.1016/j.xcrp.2021.100701

Cell Reports
Physical Science

CellPress
OPEN ACCESS

Article

Near-infrared unsymmetrical squaraine core-based sensitizers for co-sensitized high-photocurrent dye-sensitized solar cells

Jonathon Watson,[1,2] Roberta R. Rodrigues,[1,2,3] and Jared H. Delcamp[1,4,*]

SUMMARY

Increased conversion of near-infrared (NIR) photons to electricity is needed to improve dye-sensitized solar cells (DSCs). Here, we report two squaraine dyes (RR13 and RR14) with unsymmetrical cores as NIR dyes in DSCs. Both dyes feature a conjugated indolizine donor with an indoline donor on the opposite side of the squaraine core. The dyes are studied via absorption spectroscopy, computational interrogation, and electrochemical analysis. The use of the strongly donating indolizine donor results in NIR photon-to-current conversion extending beyond 800 nm on TiO_2 in DSC devices. The DSC devices were characterized by current-voltage curves, incident photon-to-current conversion efficiency measurements, and electrical impedance spectroscopy. After co-sensitized DSC device optimizations, the NIR-absorbing squaraine dyes complemented with commercial organic dyes (D35 and Y123) gave a high photocurrent output of ~21 mA/cm^2 with a PCE of 9.4%.

INTRODUCTION

Dye-sensitized solar cells (DCSs) are a practical, cost-effective alternative photovoltaic technology.[1–4] A working DSC contains a sensitizer for light absorption, a wide band-gap semiconductor to accept electrons from the photoexcited dye (usually TiO_2), and a redox shuttle (RS) to transfer electrons to the oxidized dye from a counter-electrode connected by an external circuit to the photoanode. Metal-free sensitizers are attractive due to facile spectral tunability, high molar absorptivities, and unparalleled performance in diffuse lighting environments, which is desirable for applications such as building integrated photovoltaics, tandem and multijunction devices, and self-powered Internet of Things (IoT) devices operating on indoor lighting.[5–9] Organic photosensitizers have been shown to use photons <750 nm with high-power conversion efficiencies (PCEs); however, sensitizers using photons >750 nm efficiently are rare in the literature.[10,11] This represents an urgent challenge with respect to DSC development.

Squaraine-based sensitizers are well known in the literature to absorb low-energy photons (<1.65 eV) with high molar absorptivities, which is attractive for a broad array of applications such as chemical sensing, carbon dioxide and water reduction via photocatalysis, photodetection, secure communications, bioimaging and phototherapy, and solar-to-electricity generation.[12–18] A key challenge in the DSC field is to design sensitizers with deeper near-infrared (NIR) absorption that efficiently generate electricity in this spectral region.[10,11] One approach to this challenge is to synthesize unsymmetrical squaraine sensitizers with strong electron donor functionality.[19,20] This strategy has led to some of the deepest NIR (and

[1]University of Mississippi, Department of Chemistry and Biochemistry, 481 Coulter Hall, University, MS 38677, USA

[2]These authors contributed equally

[3]Present address: Pacific Northwest National Laboratory, Institute for Integrated Catalysis, Richland, WA 99352, USA

[4]Lead contact

*Correspondence: delcamp@olemiss.edu

https://doi.org/10.1016/j.xcrp.2021.100701

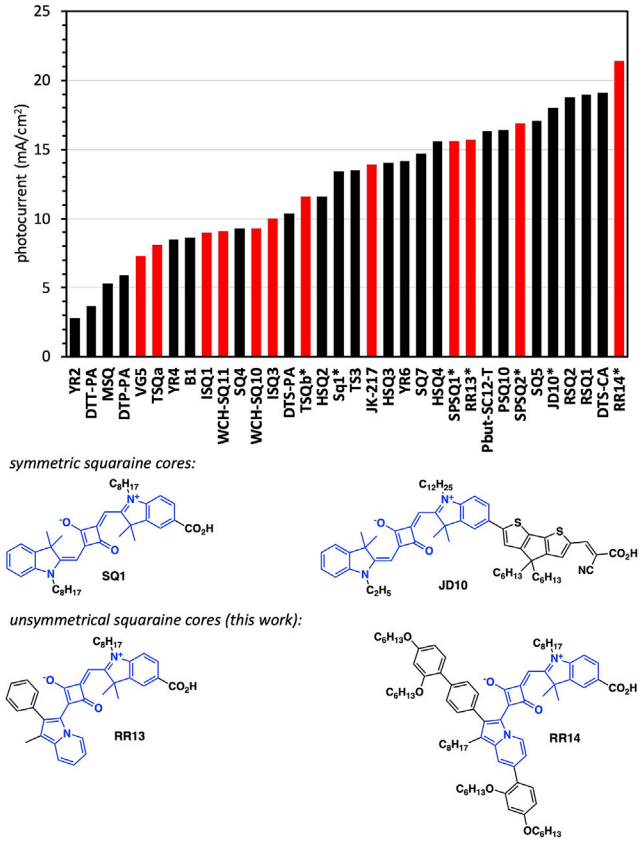

Figure 1. Photocurrent values and squaraine dyes

Top of panel shows a plot of photocurrent values observed with NIR-absorbing squaraines in DSC devices (symmetric core dyes have black bars and unsymmetrical core dyes have red bars). The asterisk indicates that the DSC device is co-sensitized. See Table S12 for a full list of dye references. The lower part of the panel provides examples of squaraine dyes in which the structures have squaraine cores in blue with functional groups in black for either anchoring (**SQ1**) or π-extending and anchoring (**JD10**) dyes. **RR13** and **RR14** have unsymmetrical squaraine cores in blue.

shortwave infrared [SWIR], >1,000 nm) photon-to-current conversion materials known in the DSC literature.[19,20] The challenge remains to design dyes that not only allow for access to the NIR/SWIR spectral regions but also have high quantum yields for electricity production from these photons.[21–25] We reasoned that an unsymmetrical squaraine core dye with a strong indolizine donor and an indoline donor with an anchoring group could shift the absorption spectrum further into the NIR region than symmetric indoline-indoline core-based squaraines. Indolizine heterocycles are fully conjugated strong donor groups with proaromatic characteristics that can enable deep NIR/SWIR absorption.[26–28] In addition, this approach will allow for the design of sensitizers that are readily accessible with concise sizes and synthetic routes, which is counter to current field trends in designing NIR chromophores.[10] Here, we report the facile preparation and application of two unsymmetrical squaraine dyes **RR13** and **RR14** in DSC devices with exceptional photocurrent outputs for squaraine-based devices (Figure 1). **RR13** features a simple, compact indolizine donor for minimal dye footprint on the TiO_2 surface. **RR14** has additional aryl ether groups to tune optical properties, reduce aggregation, and provide surface-insulating groups to protect electrons in TiO_2 from the electrolyte.[29]

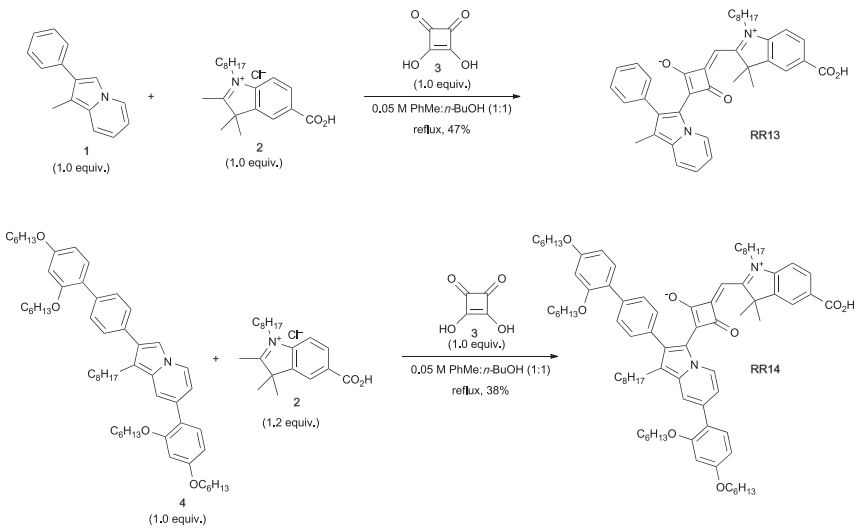

Scheme 1. Synthetic route to RR13 and RR14

RESULTS

Synthesis and optical properties of unsymmetrical squaraine core dyes

The synthesis of **RR13** occurs in 1 step via the condensation of known indolizine (**1**)[30] and carboxylated indolinium (**2**)[31] with squaric acid (**3**) to give the desired product in a 47% yield (Scheme 1). **RR14** was prepared similar to **RR13** with known indolizine (**4**)[29] in place of indolizine (**1**) to give the desired product in a 38% yield. Interestingly, **RR14** is observed to be susceptible to retro-condensation reactions, presumably due to exposure to the trace DCl in $CDCl_3$ when collecting a ^{1}H NMR spectrum with an obvious color change from the green unsymmetrical squaraine to the blue symmetric bis-indoline squaraine color (Figure S25). NMRs taken in $CDCl_3$ show a mixture consisting of ~50% **RR14** and ~25% each of the symmetrized bisindoline-squaraine/bisindolizine-squaraine dyes, despite the **RR14** sample appearing pure by chromatography before preparing the NMR sample. ^{1}H NMR spectra collected in $CDCl_3$ stored over K_2CO_3 show only **RR14** over a 24-h period (Figures S24 and S25).

Absorption spectra were obtained in dichloromethane to examine the effect of replacing an indoline with an indolizine donor (Figure 2; Table 1). Both **RR13** and **RR14** exhibit narrow absorption bands characteristic of squaraine-based sensitizers between 600 and 780 nm with absorption maxima (λ_{max}) at 689 and 712 nm, respectively. **RR14** gave the most red-shifted spectrum, with an onset of absorption (λ_{onset}) found via the 0nset program[32] at 744 nm due to the inclusion of the aryl ether donor groups in conjugation with the indolizine-squaraine π system. **RR13** and **RR14** have high molar absorptivities (ε = 166,000 M^{-1} cm^{-1} and 212,000 M^{-1} cm^{-1}, respectively) at λ_{max}, which is characteristic of squaraine sensitizers (Table 1).[21,25,33–35] Relative to symmetric squaraine core benchmark dye **SQ1**, both **RR13** and **RR14** have red-shifted λ_{max} values (by 53 and 76 nm, respectively) and larger ε values under identical conditions. These results show that the incorporation of indolizine on an unsymmetrical squaraine core has the desired shift in absorption spectrum λ_{max} values toward deeper NIR absorption. Absorption measurements of **RR13** and **RR14** on a TiO_2 surface revealed a broad absorption, which could be due to aggregation or strong absorption of the film not allowing for light transmission (Figures 2 and S5).[19,22,25] Upon the addition of chenodeoxycholic acid (CDCA) as a deaggregating agent during TiO_2 sensitization, the curve shape and breadth on TiO_2 more

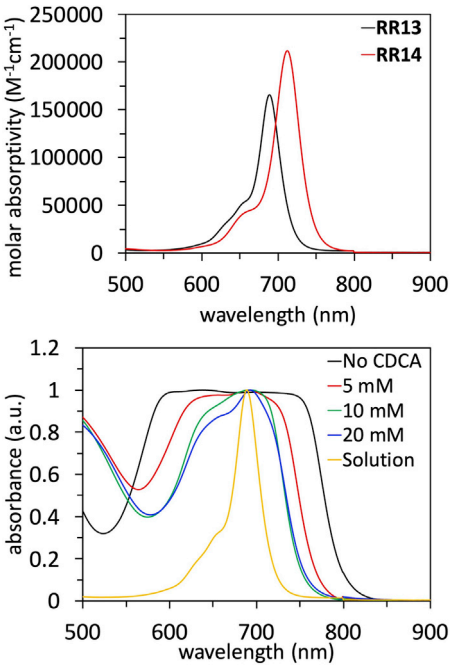

Figure 2. Absorption spectra
Absorption spectra of **RR13** and **RR14** in dichloromethane (top of panel) and normalized absorption spectra of **RR13** on TiO_2 (5 μm, 16-h sensitization time) (bottom of panel).
See Figures S5 and S6 for additional optical data.

resembles that of solution measurements, and the absorptivity is lower, which allows for light transmission during the measurements on the films studied here. Notably, when 10 mM CDCA is added to the **RR13** sensitization solution (0.1 mM dye), the full-width at half-maximum (FWHM) is 130 nm, which is significantly more than the solution measurement at 33 nm. In addition, in solution, the shoulder at 650 nm is in a 1:3 ratio with the maximum absorbance peak, while on film, the shoulder increases in height to nearly 1:1 ratio with the maximum absorbance peak. This increase in the high-energy absorption feature is indicative of aggregation such as what occurs with H-aggregates. The addition of more CDCA to the sensitization solution results in a lowering of the shoulder absorption to give a 1:1.2 ratio with the absorption maxima. This shift in the shoulder to maximum absorbance peak ratio with different CDCA loadings again suggests that aggregation may be problematic for these dyes. Similar effects are observed for **RR14** via solution and film measurements.

Density functional theory (DFT) calculations

DFT computational studies were undertaken to obtain the molecular orbital positions using the BPW91[36–38] functional and 6-311G(*d*,*p*)[39] basis set with Gaussian09 (Tables S13–S15).[40] Spatial orbital positions are critical to allow for efficient electron injection from the dye to the TiO_2 conduction band (CB) after photoexcitation and to allow for prolonged interfacial charge separation after electron injection. Ideally, the highest occupied molecular orbital (HOMO) should be far from the TiO_2 surface to inhibit back electron transfer after electron injection. Also, the lowest unoccupied molecular orbital (LUMO) should be positioned near the TiO_2 surface to allow for electron injection after excitation of an electron from the HOMO to the LUMO. **RR13** and **RR14** have delocalized HOMOs across the indolizine-squaraine core-indoline groups (Figure 3). The added aryl ether group at the 7-position of the **RR14** indolizine results in an extension of the HOMO onto the aryl ether moiety, which is correlated to the observed red-shift of its absorption spectrum. The LUMO is delocalized across the entire dye, with a slightly larger contribution on the carboxylic acid acceptor group. The presence of the LUMO near the anchoring point to TiO_2 is

Table 1. Optical and electrochemical properties of RR13 and RR14

Dye	λ_{max} (nm)	ε (M^{-1} cm^{-1})	λ_{onset} (nm)	$E_{(S+/S)}$ (V)	$E_{(S+/S^*)}$ (V)	E_g^{opt} (eV)
RR13	689	166,000	718	0.83	−0.90	1.73
RR14	712	212,000	744	0.74	−0.93	1.67

desirable for efficient electron injection. Overall, there are only minor shifts in the region of the molecule where the HOMO and LUMO are located, which indicates the HOMO to LUMO transition is of $\pi \rightarrow \pi^*$ character. This observation correlates to the observed absorption spectrum showing a high-energy shoulder feature that is assigned as vibronic in nature as is commonly observed for $\pi \rightarrow \pi^*$ transitions such as with cyanines.[41]

Time-dependent (TD)-DFT was used to evaluate the agreement between experimental absorption values and the predicted vertical transitions. TD-DFT is also used to observe which orbitals are involved in the lowest energy strong transition. The predicted vertical transition values agree closely with the experimentally obtained λ_{max} values to within 0.2 eV (Table 2). An intense (oscillator strength >1.1) vertical transition at 2.00 eV is predicted for **RR13**, which is primarily HOMO to LUMO in character (88%). Similarly, **RR14** has a predicted λ_{max} of 1.88 eV, with a higher oscillator strength (>1.4), and the transition being primarily HOMO to LUMO (89%). The higher oscillator strength of **RR14** is correlated to the observed higher ε value in solution measurements (Figure 2; Table 1).

Electrochemical properties

The thermodynamics of electron injection (ΔG_{inj}) into the TiO_2 CB and dye regeneration (ΔG_{reg}) with I^-/I_3^- were determined by electrochemical characterization. Cyclic voltammetry measurements were performed in dichloromethane solutions using 0.1 M Bu_4NPF_6 as the electrolyte and ferrocene as internal standard (Figure S2). The ground state oxidation potential ($E_{(S+/S)}$) was measured at 0.83 V versus normal hydrogen electrode (NHE) as the half-wave potential for the reversible oxidation of **RR13** (Table 1; Figure S2). As expected, the more strongly donated **RR14** is easier to oxidize with an $E_{(S+/S)}$ of 0.74 V. Notably, immobilization of the sensitizers on TiO_2 does not affect the reversibility of the oxidation wave (Figure S3). These values suggest that dye regeneration is reasonable with the I^-/I_3^- redox system, with driving forces of regeneration (ΔG_{reg}) of 480 and 390 mV when the I^-/I_3^- oxidation potential is taken at 0.35 V via the equation $\Delta G_{reg} = E_{(S+/S)} - 0.35$ V. We note that the use of 0.35 V is a gross approximation commonly used in the DSC literature[4,42–45] and that the I^-/I_3^- system is quite complex.[46,47] The excited state oxidation potential ($E_{(S+/S^*)}$) is important for characterizing the energetic driving force of electron injection (ΔG_{inj}) into TiO_2 from the photoexcited dye and is calculated using the equation $E_{(S+/S^*)} = E_{(S+/S)} - E_g^{opt}$. The E_g^{opt} values for **RR13** and **RR14** were determined from the absorption curve onset energy to be 1.73 and 1.67 eV, respectively. Both dyes give similar $E_{(S+/S^*)}$ values at −0.90 V (**RR13**) and −0.93 V (**RR14**) corresponding to ΔG_{inj} at ≥400 mV when the TiO_2 CB is taken at −0.5 V via the equation $\Delta G_{inj} = -0.5\ V - E_{(S+/S^*)}$ (Table 1; Figure S4).[4,44,48–50]

Photovoltaic performance of squaraine sensitizers in NIR-DSCs

DSC devices were prepared with both of the dyes with TiO_2 (10 μm active layer thickness) and I^-/I_3^-. The photovoltaic properties of the devices were measured by generating current density-voltage (*J-V*) curves under AM 1.5 G simulated solar illumination. Device PCEs were calculated according to the equation $PCE = (J_{SC}{*}V_{OC}{*}FF)/I_0$, where J_{SC} is the short-circuit current density, V_{OC} is the open-circuit

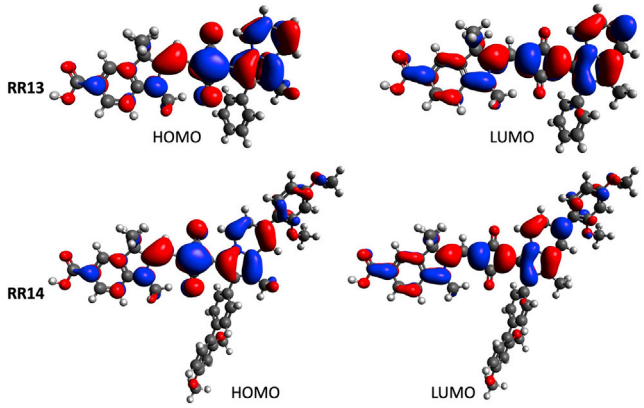

Figure 3. Frontier molecular orbitals
Frontier molecular orbital pictures for **RR13** and **RR14**.

voltage, *FF* is the fill factor, and I_0 is the incident photon flux illuminated on the cells set to 1 sun (100 mW/cm^2) unless otherwise noted. DSC devices from both **RR13** and **RR14** have low overall PCE values of 0.86% and 2.14% due primarily to low photocurrent values (<6 mA/cm^2; Table S3). Incident photon-to-current conversion efficiency (IPCE) measurements reveal IPCE peak values of <30% throughout the visible and NIR region spectral regions (Figure S10). A low IPCE response in the higher-energy visible region is noted, which agrees with the absorption spectrum. The low photocurrent and peak IPCE values are primarily attributed to detrimental aggregation at the TiO_2 surface since added CDCA improved device parameters for both dyes (Table S3). Importantly, as light-harvesting efficiency (LHE) goes down with added CDCA reducing **RR13** dye loading by almost 5 times (Figure S8; Table S1), the IPCE intensity goes up by 4 times in the NIR region (Figure S10). Similar trends are observed for **RR14**. This is an indication that aggregation is reducing IPCE efficiency, which is commonly attributed to dye-dye energy transfer resulting in annihilation, aggregate states without appropriate energetics or spatial positioning for injection, or electron transfer reactions other than dye-TiO_2 electron injection.[21,51–53] Notably, both dyes have exceptional IPCE onset values $\geq$800 nm (Figure S10). The insulating alkyl aryl ethers on the **RR14** donor led to lower CDCA loadings being required for optimized DSC device performance (Figure S10). Nonetheless, both dyes require significant CDCA loadings at up to 1:200 dye:CDCA in the case of **RR13** for optimal performances.

Squaraine dyes often have characteristically narrow absorption bands, which makes efficient panchromatic electricity generation challenging when implemented within DSC devices as single dyes due to typically low-to-moderate IPCE values (<50%) in the visible region. Recent molecular design strategies have focused on the engineering of higher energy transitions by linearly extending π-conjugation of the chromophore.[19,22–24,54] Alternatively, co-sensitization with a visible light-absorbing dye having a complementary spectrum can lead to higher-performing DSC devices.[45,55,56] An added advantage to the co-sensitization strategy is the potential use of the co-sensitizing dye as a deaggregating agent. Aggregation is often a significant concern for squaraine sensitizers due to the planarized, zwitterionic nature of the chromophores. An optically inactive co-adsorbent (CDCA) is traditionally used as a deaggregating agent. However, CDCA consumes TiO_2 binding sites with an optically inactive material in the visible spectral region, which could be better used by a visible light-absorbing dye (see Table S1 for dye loading results).[57]

Table 2. Electronic transitions

Dye	State	Orbitals	Contribution, %	Vertical transition (eV | nm)	Oscillator strength
RR13	$S_0 \rightarrow S_2$	H → L	88	2.00 | 621	1.103
RR14	$S_0 \rightarrow S_3$	H → L	89	1.88 | 660	1.455

Electronic transitions predicted by TD-DFT computation using the BPW91 functional and 6-311G(*d*,*p*) basis set. The $S_0 \rightarrow S_1$ transition for both dyes and the $S_0 \rightarrow S_2$ transition for **RR14** are very low oscillator strengths (<0.03) and are therefore not reported in the table. See Figure S9 and Table S2 for additional orbital contributions to these states and for additional transitions.

A series of co-sensitization studies were performed with well-known, visible light-absorbing commercial dyes **D35** and **Y123** to probe the possible dual role of these dyes as deaggregating agents and visible light-to-electricity-producing chromophores in DSC devices with **RR13** and **RR14** (see Figure S1 for **D35** and **Y123** structures).[58,59] The cocktail sensitizing method, in which both dyes are simultaneously present in the sensitizing solution, led to better DSC device performances in all cases compared to sequentially dipping the electrodes in single dye solutions (Figures S11–S14; Tables S4–S7).[60,61] Optimal dye ratios consisted of 1:3 NIR squaraine dye: visible light-absorbing dye, which is a drastic improvement over the required CDCA loadings for optimal PCE values. **RR13** operates more synergistically with the **D35** co-sensitizer than the **Y123** co-sensitizer, leading to a 5.3% PCE DSC device (compared to 1.9% with CDCA). The **RR13**/**D35** DSC devices more than double the photocurrent output when compared to the **RR13**/CDCA device, with the IPCE improving in both the visible range where **D35** absorbs and in the NIR region where **RR13** absorbs (Figure S11; Tables S3 and S4). **RR14** devices performed better with the **Y123** co-sensitizer, leading to a J_{SC} value of 14 mA/cm^2. The PCE of the **RR14**/**Y123** DSC device is more than double the PCE of the **RR14**/CDCA device (6.5% versus 2.9%, respectively) (Figure S12; Tables S3 and S5). The **RR14**-based DSC devices gave higher photovoltages than the **RR13**-based DSC devices due to superior surface insulation, rather than a shift in the TiO_2 capacitance, reaching a maximum V_{OC} of 708 mV, with minimal voltage losses within the cell (Figure S22; Tables S3–S5). Although device performances are comparable for **RR14** with both co-sensitizers, **Y123** is the best candidate due to better spectral matching, as evidenced in the IPCE spectra (Figures S12 and S18). Interestingly, the co-sensitizers provide the dual function of light absorbers and strong deaggregating agents, since additional CDCA loading provides no advantage with the co-sensitized systems (Figure S16).

The DSC device performances were further optimized by increasing the active photoanode thickness to 12.5 μm. The **RR13**/**D35** DSC device reaches a maximum J_{SC} value of ~16 mA/cm^2 with a PCE of 6.5% with the thicker electrodes (Figure S17; Table S9). Under these conditions, the **RR14**/**Y123** DSC device gave the highest PCE observed in these studies at 9.4%, with an exceptional J_{SC} of 21 mA/cm^2 (Figure 4; Tables 3 and S10). The IPCE shows a nearly panchromatic response from 400 to 825 nm, with a maximum of near 85% in the visible region, which is limited by the percent transmittance of the FTO used (Figures 4 and S7). The IPCE spectrum is similarly shaped with a similar percent conversion efficiency to the LHE spectrum, indicating that there is little loss of energy from the absorbed photons (Figure S8). Improved electricity production in the NIR region relative to the non-co-sensitized device is observed with a peak IPCE value of ~60% (LHE at 70% in this region) and an integrated photocurrent of 20.4 mA/cm^2 (Figure S19). This is one of the highest PCE squaraine-based devices known in the DSC literature, to the best of our knowledge, and may be one of the first squaraine-based DSC devices to reach >9.0% PCE. DSC devices with photocurrent outputs in excess of 20 mA/cm^2 are scarce for all organic DSC devices, especially without requiring significant Li

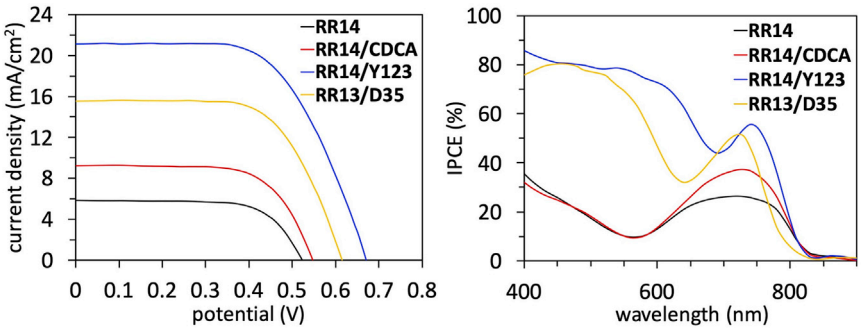

Figure 4. *J–V* and IPCE curves

J–V (left of panel) and IPCE (right of panel) curves for optimized devices with CDCA and co-sensitizer.

loadings to modulate the TiO_2 CB (Figure S15; Table S8).[62] Only 0.05 M LiI was used in these studies. Notably, minimal V_{OC} losses were observed in both co-sensitized systems not exceeding 250 mV, with the I^-/I_3^- redox system, assuming a maximum V_{OC} of ~900 mV is possible.

Electrochemical impedance spectroscopy (EIS) and small modulated photovoltage transient (SMPVT) spectroscopy

To investigate recombination kinetics for the series, EIS measurements were performed in the dark (see Figure S20 for the fitted circuit).[63] The modified Nyquist plot model shows the resistance of electron transfer at the various interfaces within the DSC, with the smaller semicircle at low resistance showing electron transfer resistance at the counter-electrode-RS interface (R_{CE}) and the larger semicircle representative of electron transfer resistance at the TiO_2-dye-RS interface (R_{rec}). Co-sensitized DSC devices show **RR14/Y123**-based devices having a desirably larger R_{rec} than **RR13/D35**-based devices (144 versus 86 Ω at V_{OC}, respectively; Table 4). This trend is observed for single-dye devices with and without CDCA (Figure S20; Table S11). These observations highlight the need for a high degree of surface protection via the insulating groups on **RR14**.[64] Both devices have characteristically low R_{CE} values for Pt and the I^-/I_3^- redox system. Charge collection efficiencies (η_{cc}) were calculated according to the equation $\eta_{cc} = 1/(1 + (R_{CE}/R_{rec}))$. A η_{cc} value of 98% is observed for the **RR14/Y123** devices. The η_{cc} value for the **RR13/D35** device is diminished to 92% (Table 4), which is correlated to the lack of surface-protecting insulating groups on the **RR13** indolizine motif.

Electron lifetimes in the TiO_2 semiconductor (τ_{TiO2}) were measured via Bode plots in the dark at V_{OC} bias and described by the equation $\tau_{TiO2} = 1/(2\pi f)$, where f is the peak frequency value in the low-frequency region of the plot (Figures 5 and S20). The **RR14/Y123** system shows a higher τ_{TiO2} value when compared to **RR13/D35** and standalone **Y123** devices (63 ms versus 32 ms and 40 ms, respectively; Tables 4 and S11). In addition, SMPVT measurements were undertaken to probe the electron lifetime in TiO_2 under steady-state illumination via measurement of the fitted lifetimes of the rise and decay in V_{OC} induced by small changes in light intensity (Figure S21).[65,66] **RR14/Y123** devices show nearly an order of magnitude longer electron lifetime in TiO_2 when compared to **RR13/D35** at that same V_{OC} value. Maximum electron lifetimes as high as 0.1 s are observed for the **RR14/Y123**-based DSC devices. A longer electron lifetime with **RR14**-based cells is observed when compared to **RR13**-based cells both with and without CDCA (Figure S21). Thus, the EIS and SMPVT measurements under 2 separate conditions (dark and light environments)

Table 3. Optimized DSC device data

Dye	V_{oc} (mV)	J_{sc} (mA/cm^2)	FF (%)	PCE (%)
RR13	467 ± 10	4.0 ± 0	69.8 ± 3.3	1.40 ± 0.10
RR13/CDCA	527 ± 5	7.6 ± 0.1	74.5 ± 0.1	3.22 ± 0.06
RR13/D35	612 ± 5	15.7 ± 0	63.3 ± 1.6	6.52 ± 0.21
RR14	523 ± 0	5.8 ± 0.1	68.4 ± 0.7	2.31 ± 0.04
RR14/CDCA	548 ± 5	9.0 ± 0.5	67.6 ± 1.0	3.68 ± 0.11
RR14/Y123	662 ± 5	20.9 ± 0.7	61.4 ± 0.9	9.44 ± 0.24

both suggest that the surface-insulating groups on the **RR14** dye are critical to long-lived electrons in TiO_2, which is correlated to the higher photovoltage observed with the **RR14**-based DSC devices that leads to significantly higher power conversion efficiencies than **RR13**-based DSC devices.

DISCUSSION

Two unsymmetrical indolizine-squaraine-indoline-based sensitizers, **RR13** and **RR14**, were synthesized and characterized in solution and in DSC devices. The sensitizers exhibited strong NIR absorption extending to 800 nm on a TiO_2 surface. Electrochemical and optical analysis reveals that both sensitizers are well suited for use in DSC devices energetically. Computational studies show good orbital distribution on the dyes for electron injection into TiO_2. On TiO_2, aggregation-induced absorption was correlated to diminished DSC device performances for both dyes with CDCA deaggregation studies showing high CDCA loadings (>50:1 CDCA:dye) having optimal performances. To address both the minimal light absorption in the visible region of the dyes and the aggregated squaraine dyes on the surface, co-sensitizers working in the visible region of the spectrum were added to the DSC devices in place of CDCA. This strategy reduces the need to design a single chromophore for panchromatic collection of solar energy and improves the current output by the removal of CDCA. The highest performing device was based on co-sensitized dyes **RR14/Y123** resulting in a PCE value of 9.4%, with a J_{SC} value of 21 mA/cm^2. To the best of our knowledge, this is the highest performing squaraine-based device in the DSC literature. Minimal photovoltage loss is present in these DSC devices due to excellent surface insulation of electrons in TiO_2 from the electrolyte by the alkyl groups on the dye, as confirmed by EIS and SMPVT measurements. Given the very low Li loadings (0.05 M Li^+) and high photocurrent density with NIR light use, the **RR14/Y123** dye system is a good candidate for use in sequential series multijunction (SSM) DSC systems as the long wavelength-using material. Future studies will focus on identifying energetically well-paired redox shuttles for NIR DSCs, SSM-DSCs, and low-light DSC applications.

EXPERIMENTAL PROCEDURES

Resource availability

Lead contact

Further information and requests for resources and reagents should be directed to and will be fulfilled by the lead contact, Jared H. Delcamp (delcamp@olemiss.edu).

Table 4. EIS data summary for the optimized co-sensitized devices

Dye	R_s, Ω	R_{rec}, Ω	C_μ, mF	R_{CE}, Ω	C_{CE}, mF	η_{cc}, %	τ_{TiO2}, ms
RR13/D35	14	86	7.5×10^{-4}	7	4.8×10^{-6}	92	32
RR14/Y123	17	144	1.2×10^{-3}	3	2.6×10^{-5}	98	63

R_S, series resistance; C_μ, chemical capacitance for charge accumulation at the photoanode; C_{CE}, capacitance at the electrolyte-counter electrode interface.

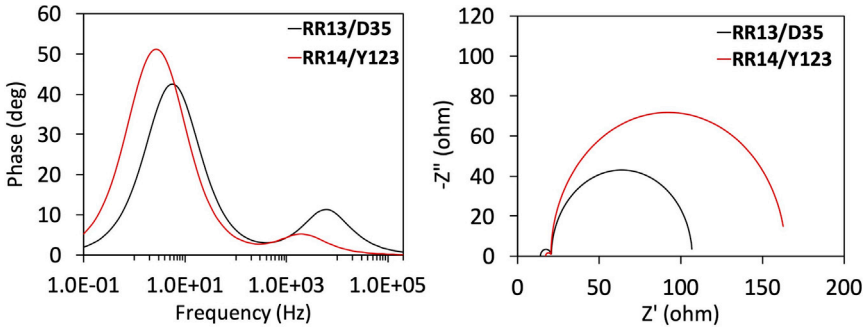

Figure 5. EIS data

EIS data for optimized co-sensitized devices. Bode plot (left of panel) and Nyquist plot (right of panel). See Figure S20 and Table S11 for additional EIS data.

Materials availability

The dyes synthesized for these studies may be available from the lead contact upon request as supplies are available.

Data and code availability

All data generated for this study are included in this article or the supplemental information. This study did not generate code.

General procedures

All commercially obtained reagents were used as received. Full descriptions of the synthesis and characterization, computational methods, instrumentation, and device fabrication can be found in Notes S1–S3.

SUPPLEMENTAL INFORMATION

Supplemental information can be found online at https://doi.org/10.1016/j.xcrp.2021.100701.

ACKNOWLEDGMENTS

These studies were funded through National Science Foundation (NSF) award 1954922 and NSF supplementary award 2111582.

AUTHOR CONTRIBUTIONS

R.R. synthesized and characterized the dyes and performed preliminary device studies for the series. J.W. performed DFT calculations, additional dye characterization, device fabrication/characterization, and wrote the original manuscript draft. J.H.D. conceived the project, oversaw the research, and wrote the final draft of the manuscript.

DECLARATION OF INTERESTS

J.H.D. is an inventor on a patent application filed by the University of Mississippi related to the dyes in this work.

Received: June 25, 2021
Revised: September 23, 2021
Accepted: December 3, 2021
Published: December 29, 2021

REFERENCES

1. Fakharuddin, A., Jose, R., Brown, T.M., Fabregat-Santiago, F., and Bisquert, J. (2014). A perspective on the production of dye-sensitized solar modules. Energy Environ. Sci. *7*, 3952–3981.

2. Polman, A., Knight, M., Garnett, E.C., Ehrler, B., and Sinke, W.C. (2016). Photovoltaic materials: present efficiencies and future challenges. Science *352*, aad4424.

3. Saifullah, M., Gwak, J., and Yun, J.H. (2016). Comprehensive review on material requirements, present status, and future prospects for building-integrated semitransparent photovoltaics (BISTPV). J. Mater. Chem. A Mater. Energy Sustain. *4*, 8512–8540.

4. Hagfeldt, A., Boschloo, G., Sun, L., Kloo, L., and Pettersson, H. (2010). Dye-sensitized solar cells. Chem. Rev. *110*, 6595–6663.

5. Freitag, M., Teuscher, J., Saygili, Y., Zhang, X., Giordano, F., Liska, P., Hua, J., Zakeeruddin, S.M., Moser, J.-E., Grätzel, M., and Hagfeldt, A. (2017). Dye-sensitized solar cells for efficient power generation under ambient lighting. Nat. Photonics *11*, 372–378.

6. Aslam, A., Mehmood, U., Arshad, M.H., Ishfaq, A., Zaheer, J., Ul Haq Khan, A., and Sufyan, M. (2020). Dye-sensitized solar cells (DSSCs) as a potential photovoltaic technology for the self-powered internet of things (IoTs) applications. Sol. Energy *207*, 874–892.

7. Michaels, H., Rinderle, M., Freitag, R., Benesperi, I., Edvinsson, T., Socher, R., Gagliardi, A., and Freitag, M. (2020). Dye-sensitized solar cells under ambient light powering machine learning: towards autonomous smart sensors for the internet of things. Chem. Sci. (Camb.) *11*, 2895–2906.

8. Cheema, H., Watson, J., and Delcamp, J.H. (2021). Integrating GaAs, Si, and Dye-Sensitized Solar Cells in Multijunction Devices and Probing Harsh Condition Behavior. ACS Appl. Electron. Mater. *3*, 316–324.

9. Zhang, D., Stojanovic, M., Ren, Y., Cao, Y., Eickemeyer, F.T., Socie, E., Vlachopoulos, N., Moser, J.-E., Zakeeruddin, S.M., Hagfeldt, A., and Grätzel, M. (2021). A molecular photosensitizer achieves a V_{oc} of 1.24 V enabling highly efficient and stable dye-sensitized solar cells with copper(II/I)-based electrolyte. Nat. Commun. *12*, 1777.

10. Brogdon, P., Cheema, H., and Delcamp, J.H. (2018). Near-Infrared-Absorbing Metal-Free Organic, Porphyrin, and Phthalocyanine Sensitizers for Panchromatic Dye-Sensitized Solar Cells. ChemSusChem *11*, 86–103.

11. Hardin, B.E., Snaith, H.J., and McGehee, M.D. (2012). The renaissance of dye-sensitized solar cells. Nat. Photonics *6*, 162–169.

12. Chen, G., Sasabe, H., Igarashi, T., Hong, Z., and Kido, J. (2015). Squaraine dyes for organic photovoltaic cells. J. Mater. Chem. A Mater. Energy Sustain. *3*, 14517–14534.

13. Xia, G., and Wang, H. (2017). Squaraine dyes: the hierarchical synthesis and its application in optical detection. J. Photochem. Photobiol. Photochem. Rev. *31*, 84–113.

14. He, J., Jo, Y.J., Sun, X., Qiao, W., Ok, J., Kim, T.i., and Li, Z. (2020). Squaraine Dyes for Photovoltaic and Biomedical Applications. Adv. Funct. Mater. *31*, 2008201.

15. Ilina, K., MacCuaig, W.M., Laramie, M., Jeouty, J.N., McNally, L.R., and Henary, M. (2020). Squaraine Dyes: Molecular Design for Different Applications and Remaining Challenges. Bioconjug. Chem. *31*, 194–213.

16. Yao, D., Wang, Y., Zou, R., Bian, K., Liu, P., Shen, S., Yang, W., Zhang, B., and Wang, D. (2020). Molecular Engineered Squaraine Nanoprobe for NIR-II/Photoacoustic Imaging and Photothermal Therapy of Metastatic Breast Cancer. ACS Appl. Mater. Interfaces *12*, 4276–4284.

17. Strassel, K., Hu, W.-H., Osbild, S., Padula, D., Rentsch, D., Yakunin, S., Shynkarenko, Y., Kovalenko, M., Nüesch, F., Hany, R., and Bauer, M. (2021). Shortwave infrared-absorbing squaraine dyes for all-organic optical upconversion devices. Sci. Technol. Adv. Mater. *22*, 194–204.

18. Jo, M., Choi, S., Jo, J.H., Kim, S.-Y., Kim, P.S., Kim, C.H., Son, H.-J., Pac, C., and Kang, S.O. (2019). Utility of Squaraine Dyes for Dye-Sensitized Photocatalysis on Water or Carbon Dioxide Reduction. ACS Omega *4*, 14272–14283.

19. Bisht, R., Mele Kavungathodi, M.F., and Nithyanandhan, J. (2018). Indenoquinaldine-Based Unsymmetrical Squaraine Dyes for Near-Infrared Absorption: Investigating the Steric and Electronic Effects in Dye-Sensitized Solar Cells. Chemistry *24*, 16368–16378.

20. Li, J.-Y., Chen, C.-Y., Ho, W.-C., Chen, S.-H., and Wu, C.-G. (2012). Unsymmetrical squaraines incorporating quinoline for near infrared responsive dye-sensitized solar cells. Org. Lett. *14*, 5420–5423.

21. Alagumalai, A., M k, M.F., Vellimalai, P., Sil, M.C., and Nithyanandhan, J. (2016). Effect of Out-of-Plane Alkyl Group's Position in Dye-Sensitized Solar Cell Efficiency: A Structure-Property Relationship Utilizing Indoline-Based Unsymmetrical Squaraine Dyes. ACS Appl. Mater. Interfaces *8*, 35353–35367.

22. Delcamp, J.H., Shi, Y., Yum, J.-H., Sajoto, T., Dell'Orto, E., Barlow, S., Nazeeruddin, M.K., Marder, S.R., and Grätzel, M. (2013). The role of π bridges in high-efficiency DSCs based on unsymmetrical squaraines. Chemistry *19*, 1819–1827.

23. Jradi, F.M., Kang, X., O'Neil, D., Pajares, G., Getmanenko, Y.A., Szymanski, P., Parker, T.C., El-Sayed, M.A., and Marder, S.R. (2015). Near-Infrared Asymmetrical Squaraine Sensitizers for Highly Efficient Dye Sensitized Solar Cells: The Effect of π-Bridges and Anchoring Groups on Solar Cell Performance. Chem. Mater. *27*, 2480–2487.

24. Jradi, F.M., O'Neil, D., Kang, X., Wong, J., Szymanski, P., Parker, T.C., Anderson, H.L., El-Sayed, M.A., and Marder, S.R. (2015). A Step Toward Efficient Panchromatic Multi-Chromophoric Sensitizers for Dye Sensitized Solar Cells. Chem. Mater. *27*, 6305–6313.

25. Bisht, R., M k, M.F., Singh, A.K., and Nithyanandhan, J. (2017). Panchromatic Sensitizer for Dye-Sensitized Solar Cells: Unsymmetrical Squaraine Dyes Incorporating Benzodithiophene π-Spacer with Alkyl Chains to Extend Conjugation, Control the Dye Assembly on TiO_2, and Retard Charge Recombination. J. Org. Chem. *82*, 1920–1930.

26. Huckaba, A.J., Yella, A., McNamara, L.E., Steen, A.E., Murphy, J.S., Carpenter, C.A., et al. (2016). Molecular Design Principles for Near-Infrared Absorbing and Emitting Indolizine Dyes. Chem. Eur. J. *22*, 15536–15542.

27. Gayton, J., Autry, S.A., Meador, W., Parkin, S.R., Hill, G.A., Jr., Hammer, N.I., and Delcamp, J.H. (2019). Indolizine-Cyanine Dyes: Near Infrared Emissive Cyanine Dyes with Increased Stokes Shifts. J. Org. Chem. *84*, 687–697.

28. Rathnamalala, C.S.L., Gayton, J.N., Dorris, A.L., Autry, S.A., Meador, W., Hammer, N.I., Delcamp, J.H., and Scott, C.N. (2019). Donor-Acceptor-Donor NIR II Emissive Rhodindolizine Dye Synthesized by C-H Bond Functionalization. J. Org. Chem. *84*, 13186–13193.

29. Huckaba, A.J., Yella, A., Brogdon, P., Scott Murphy, J., Nazeeruddin, M.K., Grätzel, M., and Delcamp, J.H. (2016). A low recombination rate indolizine sensitizer for dye-sensitized solar cells. Chem. Commun. (Camb.) *52*, 8424–8427.

30. Huckaba, A.J., Giordano, F., McNamara, L.E., Dreux, K.M., Hammer, N.I., Tschumper, G.S., Zakeeruddin, S.M., Grätzel, M., Nazeeruddin, M.K., and Delcamp, J.H. (2015). Indolizine-Based Donors as Organic Sensitizer Components for Dye-Sensitized Solar Cells. Adv. Energy Mater. *5*, 1401629.

31. Choi, H., Kim, S., Kang, S.O., Ko, J., Kang, M.-S., Clifford, J.N., Forneli, A., Palomares, E., Nazeeruddin, M.K., and Grätzel, M. (2008). Stepwise cosensitization of nanocrystalline TiO_2 films utilizing Al_2O_3 layers in dye-sensitized solar cells. Angew. Chem. Int. Ed. Engl. *47*, 8259–8263.

32. Wallace, A.M., Curiac, C., Delcamp, J.H., and Fortenberry, R.C. (2021). Accurate determination of the onset wavelength (λ_{onset}) in optical spectroscopy. J. Quant. Spectrosc. Radiat. Transf. *265*, 107544.

33. Punitharasu, V., Mele Kavungathodi, M.F., Singh, A.K., and Nithyanandhan, J. (2019). π-Extended cis-Configured Unsymmetrical Squaraine Dyes for Dye-Sensitized Solar Cells: Panchromatic Response. ACS Appl. Energy Mater. *2*, 8464–8472.

34. Paek, S., Choi, H., Kim, C., Cho, N., So, S., Song, K., Nazeeruddin, M.K., and Ko, J. (2011). Efficient and stable panchromatic squaraine dyes for dye-sensitized solar cells. Chem. Commun. (Camb.) *47*, 2874–2876.

35. Rao, G.H., Venkateswararao, A., Giribabu, L., Han, L., Bedja, I., Gupta, R.K., Islam, A., and Singh, S.P. (2016). Near-infrared squaraine co-sensitizer for high-efficiency dye-sensitized solar cells. Phys. Chem. Chem. Phys. *18*, 14279–14285.

36. Yum, J.-H., Walter, P., Huber, S., Rentsch, D., Geiger, T., Nüesch, F., De Angelis, F., Grätzel, M., and Nazeeruddin, M.K. (2007). Efficient far red sensitization of nanocrystalline TiO_2 films by an unsymmetrical squaraine dye. J. Am. Chem. Soc. *129*, 10320–10321.

37. Becke, A.D. (1988). Density-functional exchange-energy approximation with correct asymptotic behavior. Phys. Rev. A Gen. Phys. *38*, 3098–3100.

38. Perdew, J.P., and Wang, Y. (1992). Accurate and simple analytic representation of the electron-gas correlation energy. Phys. Rev. B Condens. Matter *45*, 13244–13249.

39. Frisch, M.J., Pople, J.A., and Binkley, J.S. (1984). Self-consistent molecular orbital methods 25. Supplementary functions for Gaussian basis sets. J. Chem. Phys. *80*, 3265–3269.

40. Frisch, M.J., Trucks, G.W., Schlegel, H.B., Scurseria, G.E., Robb, M.A., Cheeseman, J.R., Scalmani, G., Barone, V., Mennucci, B., Petersson, A., et al. (2009). Gaussian09 Revision E.01 (Gaussian).

41. Mustroph, H., and Towns, A. (2018). Fine Structure in Electronic Spectra of Cyanine Dyes: Are Sub-Bands Largely Determined by a Dominant Vibration or a Collection of Singly Excited Vibrations? ChemPhysChem *19*, 1016–1023.

42. Sun, Z., Liang, M., and Chen, J. (2015). Kinetics of Iodine-Free Redox Shuttles in Dye-Sensitized Solar Cells: Interfacial Recombination and Dye Regeneration. Acc. Chem. Res. *48*, 1541–1550.

43. Pashaei, B., Shahroosvand, H., and Abbasi, P. (2015). Transition metal complex redox shuttles for dye-sensitized solar cells. RSC Advances *5*, 94814–94848.

44. Anderson, A.Y., Barnes, P.R.F., Durrant, J.R., and O'Regan, B.C. (2011). Quantifying Regeneration in Dye-Sensitized Solar Cells. J. Phys. Chem. C *115*, 2439–2447.

45. Cole, J.M., Pepe, G., Al Bahri, O.K., and Cooper, C.B. (2019). Cosensitization in Dye-Sensitized Solar Cells. Chem. Rev. *119*, 7279–7327.

46. Boschloo, G., and Hagfeldt, A. (2009). Characteristics of the iodide/triiodide redox mediator in dye-sensitized solar cells. Acc. Chem. Res. *42*, 1819–1826.

47. Ardo, S., and Meyer, G.J. (2009). Photodriven heterogeneous charge transfer with transition-metal compounds anchored to TiO_2 semiconductor surfaces. Chem. Soc. Rev. *38*, 115–164.

48. Urbani, M., Grätzel, M., Nazeeruddin, M.K., and Torres, T. (2014). Meso-substituted porphyrins for dye-sensitized solar cells. Chem. Rev. *114*, 12330–12396.

49. Mishra, A., Fischer, M.K.R., and Bäuerle, P. (2009). Metal-free organic dyes for dye-sensitized solar cells: from structure: property relationships to design rules. Angew. Chem. Int. Ed. Engl. *48*, 2474–2499.

50. Ronca, E., Pastore, M., Belpassi, L., Tarantelli, F., and De Angelis, F. (2013). Influence of the dye molecular structure on the TiO_2 conduction band in dye-sensitized solar cells: disentangling charge transfer and electrostatic effects. Energy Environ. Sci. *6*, 183–193.

51. de Miguel, G., Marchena, M., Ziółek, M., Pandey, S.S., Hayase, S., and Douhal, A. (2012). Femto- to Millisecond Photophysical Characterization of Indole-Based Squaraines Adsorbed on TiO_2 Nanoparticle Thin Films. J. Phys. Chem. C *116*, 12137–12148.

52. Zeng, K., Lu, Y., Tang, W., Zhao, S., Liu, Q., Zhu, W., Tian, H., and Xie, Y. (2018). Efficient solar cells sensitized by a promising new type of porphyrin: dye-aggregation suppressed by double strapping. Chem. Sci. (Camb.) *10*, 2186–2192.

53. Higgins, G.T., Bergeron, B.V., Hasselmann, G.M., Farzad, F., and Meyer, G.J. (2006). Intermolecular energy transfer across nanocrystalline semiconductor surfaces. J. Phys. Chem. B *110*, 2598–2605.

54. Maeda, T., Arikawa, S., Nakao, H., Yagi, S., and Nakazumi, H. (2013). Linearly π-extended squaraine dyes enable the spectral response of dye-sensitized solar cells in the NIR region over 800 nm. New J. Chem. *37*, 701–708.

55. Zeng, K., Chen, Y., Zhu, W.-H., Tian, H., and Xie, Y. (2020). Efficient Solar Cells Based on Concerted Companion Dyes Containing Two Complementary Components: An Alternative Approach for Cosensitization. J. Am. Chem. Soc. *142*, 5154–5161.

56. Zhang, W., Li, W., Wu, Y., Liu, J., Song, X., Tian, H., and Zhu, W.-H. (2016). Novel Squaraine Cosensitization System of Panchromatic Light-Harvesting with Synergistic Effect for Highly Efficient Solar Cells. ACS Sustain. Chem.& Eng. *4*, 3567–3574.

57. Lee, K.-M., Chen, C.-Y., Wu, S.-J., Chen, S.-C., and Wu, C.-G. (2013). Surface passivation: the effects of CDCA co-adsorbent and dye bath solvent on the durability of dye-sensitized solar cells. Sol. Energy Mater. Sol. Cells *108*, 70–77.

58. Feldt, S.M., Gibson, E.A., Gabrielsson, E., Sun, L., Boschloo, G., and Hagfeldt, A. (2010). Design of organic dyes and cobalt polypyridine redox mediators for high-efficiency dye-sensitized solar cells. J. Am. Chem. Soc. *132*, 16714–16724.

59. Tsao, H.N., Yi, C., Moehl, T., Yum, J.-H., Zakeeruddin, S.M., Nazeeruddin, M.K., and Grätzel, M. (2011). Cyclopentadithiophene bridged donor-acceptor dyes achieve high power conversion efficiencies in dye-sensitized solar cells based on the tris-cobalt bipyridine redox couple. ChemSusChem *4*, 591–594.

60. Wu, H.-P., Ou, Z.-W., Pan, T.-Y., Lan, C.-M., Huang, W.-K., Lee, H.-W., Reddy, N.M., Chen, C.-T., Chao, W.-S., Yeh, C.-Y., and Diau, E.W.-G. (2012). Molecular engineering of cocktail co-sensitization for efficient panchromatic porphyrin-sensitized solar cells. Energy Environ. Sci. *5*, 9483–9848.

61. Fan, S., Lu, X., Sun, H., Zhou, G., Chang, Y.J., and Wang, Z.S. (2016). Effect of the co-sensitization sequence on the performance of dye-sensitized solar cells with porphyrin and organic dyes. Phys. Chem. Chem. Phys. *18*, 932–938.

62. Jennings, J.R., and Wang, Q. (2010). Influence of Lithium Ion Concentration on Electron Injection, Transport, and Recombination in Dye-Sensitized Solar Cells. J. Phys. Chem. C *114*, 1715–1724.

63. Wang, Q., Moser, J.-E., and Grätzel, M. (2005). Electrochemical impedance spectroscopic analysis of dye-sensitized solar cells. J. Phys. Chem. B *109*, 14945–14953.

64. Baumann, A., Curiac, C., and Delcamp, J.H. (2020). The Hagfeldt Donor and Use of Next-Generation Bulky Donor Designs in Dye-Sensitized Solar Cells. ChemSusChem *13*, 2503–2512.

65. Boschloo, G., Häggman, L., and Hagfeldt, A. (2006). Quantification of the effect of 4-*tert*-butylpyridine addition to I^-/I_3^- redox electrolytes in dye-sensitized nanostructured TiO_2 solar cells. J. Phys. Chem. B *110*, 13144–13150.

66. Nissfolk, J., Fredin, K., Hagfeldt, A., and Boschloo, G. (2006). Recombination and transport processes in dye-sensitized solar cells investigated under working conditions. J. Phys. Chem. B *110*, 17715–17718.